Computational tool to study perturbations in muscle regulation and its application to heart disease

Samantha K. Barrick[1,2], Sarah R. Clippinger[1,2], Lina Greenberg[1], Michael J. Greenberg[1,*]

[1] Department of Biochemistry and Molecular Biophysics, Washington University School of Medicine, St. Louis, MO, 63110, USA

[2] These authors contributed equally to this work

[*]Corresponding author:
Michael J. Greenberg
Department of Biochemistry and Molecular Biophysics
Washington University School of Medicine
660 S. Euclid Ave., Campus Box 8231
St. Louis, MO 63110
Phone: (314) 362-8670
Email: greenberg@wustl.edu

Running title: Tool for studying thin-filament regulation

Keywords: Cardiomyopathies, thin filament, myosin

Abstract

Striated muscle contraction occurs when myosin thick filaments bind to thin filaments in the sarcomere and generate pulling forces. This process is regulated by calcium, and it can be perturbed by pathological conditions (e.g., myopathies), physiological adaptations (e.g., β-adrenergic stimulation), and pharmacological interventions. Therefore, it is important to have a methodology to robustly determine the mechanism of these perturbations and statistically evaluate their effects. Here, we present an approach to measure the equilibrium constants that govern muscle activation, estimate uncertainty in these parameters, and statistically test the effects of perturbations. We provide a MATLAB-based computational tool for these analyses, along with easy-to-follow tutorials that make this approach accessible. The hypothesis testing and error estimation approaches described here are broadly applicable, and the provided tools work with other types of data, including cellular measurements. To demonstrate the utility of the approach, we apply it to determine the biophysical mechanism of a mutation that causes familial hypertrophic cardiomyopathy. This approach is generally useful for studying the mechanisms of muscle diseases and therapeutic interventions that target muscle contraction.

Introduction

Force production in cardiac and skeletal muscle is tightly regulated to ensure that contraction occurs in a controlled and concerted manner. Dysfunction of this regulation can lead to a wide array of diseases, including cardiomyopathies, and there are currently several therapies in development that target this regulation (1-3). Given the role of perturbations of muscle regulation in health and disease, there is an outstanding need for tools that can resolve statistically significant changes in this regulation.

At the molecular scale, force production in muscle is powered by the molecular motor myosin, which contracts the sarcomere by pulling thin filaments (i.e., actin filaments decorated with tropomyosin and the troponin complex) toward the M-line of the sarcomere. The interaction between myosin and the thin filament is regulated in a calcium-dependent manner, where calcium influx into the cytoplasm leads to activation of the thin filament and subsequent muscle contraction. In their landmark work, McKillop and Geeves (4) used a battery of biochemical and biophysical techniques to demonstrate that thin-filament activation is a multi-step process, requiring contributions from calcium binding to troponin as well as actomyosin binding. Their model is known as the “three-state model” (Fig. 1). In the absence of calcium, tropomyosin is in the blocked state, obscuring the myosin-binding site on the thin filament and inhibiting muscle contraction. Calcium binding to the troponin complex causes tropomyosin to shift to the closed state on the thin filament, exposing part of the myosin-binding site. Tropomyosin can either move to the open position spontaneously, where it permits myosin strong binding, or it can be pushed there by myosin binding. Myosin first binds weakly to the thin filament, then isomerizes to a strongly bound, force-generating state. The binding of one myosin

66 to the thin filament pushes tropomyosin into the open position, exposing adjacent myosin-
67 binding sites and leading to cooperative activation. The three states of tropomyosin
68 positioning along the thin filament were subsequently confirmed using structural
69 techniques (5).

70 The three-state model provides a useful framework to understand the mechanism
71 of perturbations in skeletal and cardiac thin-filament regulation, such as drug treatments
72 (1, 6), protein isoform changes (7), disease-causing mutations (8), and post-translational
73 modifications (9, 10). The formalism laid out by McKillop and Geeves enables the
74 determination of the equilibrium constants that govern transitions between states, and
75 thus the population of thin-filament regulatory units in each state (Fig. 1). However, it has
76 been challenging to precisely define the values of these equilibrium constants, due in part
77 to the number of free parameters in the model. Furthermore, the original McKillop and
78 Geeves approach did not provide a methodology for assessment of uncertainty in
79 parameter values or hypothesis testing. Such a methodology is necessary for the rigorous
80 assessment of the effects of perturbations.

81 Here, we have modified the approach of McKillop and Geeves to better resolve the
82 effects of perturbations in tropomyosin positioning along the thin filament. We provide a
83 MATLAB-based computational tool and a user guide that enables users to measure the
84 equilibrium constants that govern thin-filament activation, estimate uncertainty in these
85 parameters, and statistically test the effects of perturbations. We demonstrate the utility
86 of our approach by applying it to determine the biophysical mechanism of a mutation in
87 troponin T, ΔE160, that causes familial hypertrophic cardiomyopathy (HCM) (11). This
88 approach allows for the robust determination of differences between wild-type and mutant

89 proteins, which is an important step toward developing novel therapies to treat HCM and

90 other devastating muscle diseases.

91

Materials and Methods

Determination of equilibrium constants using the McKillop and Geeves analysis

In the classic McKillop and Geeves analysis, the values of the equilibrium constants that govern muscle activation (Fig. 1) were determined from biochemical measurements. K_B was calculated based on stopped-flow measurement of the rate of myosin binding to regulated thin filaments (RTFs) (see Supporting Materials for details). K_W, K_T, and nH (i.e., the size of the cooperative unit) were calculated from titrations of pyrene-labeled RTFs with myosin performed at saturating calcium (pCa 3) and in the absence of calcium (2 mM EGTA) (see Supporting Materials for details). The relationship between the fraction of myosin-bound subunits, $f([m])$, and the fractional change in pyrene fluorescence upon myosin binding is given by the following equation (4):

$$f([m]) = \frac{F_0 - F}{F_0 - F_\infty} = \frac{K_W[m]P^{(nH-1)}(K_T(1+K_S)^{(nH)}+1)}{\left(K_T P^{(nH)} + Q^{(nH)} + \frac{1}{K_B}\right)(1+K_S)^{(nH-1)}} \qquad \text{Equation 1}$$

where F is the measured pyrene fluorescence; F_0 and F_∞ are the pyrene fluorescence in the absence of myosin and at saturating myosin, respectively; [m] is the concentration of myosin; $P = 1 + [m]*K_W(1 + K_S)$; and $Q = 1 + [m]*K_W$. K_B at high calcium and K_S were set to 20 and 18, respectively, based on (4). nH, K_W, and K_T were determined in the presence and absence of calcium by fitting each titration curve independently.

Modified fitting approach

To improve the resolution of the parameters extracted from fitting of the data, we modified the classic McKillop and Geeves approach:

(1) We performed an additional titration at an intermediate calcium concentration (pCa 6.25).

115 (2) The data for curves collected at three different calcium concentrations were
116 globally fit using least squares optimization, and the parameters that minimized the
117 aggregate error in all three data sets were determined. In global fitting, individual
118 parameters can be shared between data sets, reducing the number of free
119 variables and increasing the power to precisely measure parameter values. Here,
120 K_W and *nH* were shared parameters among all three curves; however, this
121 approach does not require sharing these parameters.
122 (3) We used an annealing routine in our fitting procedure to avoid biasing the
123 fit toward the initial guesses used in the fitting. The annealing routine ensures that
124 the best-fit parameters are obtained from a global rather than local minimum.
125
126 **Hypothesis testing and statistics**
127 One limitation of the original formulation of the three-state model is that it lacks
128 procedures for calculating uncertainties and statistical hypothesis testing. Here, we used
129 the well-established technique of bootstrapping simulations to calculate 95% confidence
130 intervals (12, 13). In the bootstrapping method, the original data set is randomly
131 resampled to generate synthetic data sets, each containing the same number of points
132 as the original data set. Each synthetic data set is then fit to determine the best-fit values
133 of the parameters for that data set. 95% confidence intervals are defined as the interval
134 over which 95% of the simulated parameter values are found. Note that the number of
135 bootstrapping simulations required will depend on the noise in the data as well as the
136 number of sampled points. As such, one should empirically determine the number of
137 simulations required for stable convergence of the confidence intervals. We have found

138 that for the experiments described here, 1000 rounds of bootstrapping simulations were
139 sufficient (Fig. 2A).

140 For statistical hypothesis testing, we defined a test statistic as the difference
141 between parameter values in the perturbed and unperturbed systems (14). For example,
142 to determine whether there is a statistically significant difference in the value of K_W for a
143 mutant protein relative to wild-type (WT), the test statistic is $H = K_W(WT) - K_W(mutant)$.
144 The value of the test statistic is calculated for the real data and for pairs of K_W values
145 drawn from the bootstrapping simulations of the data. The interval within which 95% of
146 the test statistic values from the bootstrapped simulations fall is defined as the 95%
147 confidence interval. If the null hypothesis (i.e., $H_0=0$) is not contained within the 95%
148 confidence interval, then the null hypothesis is rejected, and $K_W(WT) \neq K_W(mutant)$ with a
149 p-value < 0.05 (Fig. 2B-C). The p-value can be calculated from a cumulative distribution
150 of the test statistic by finding the largest interval that does not contain the null hypothesis
151 (Fig. 2D). This value is multiplied by two to make the test equivalent to a two-tailed test.
152

Results and Discussion

Here we present a methodology and MATLAB-based computational tool for analyzing biochemical measurements of thin-filament positioning. This procedure builds on the formalism developed by McKillop and Geeves (4), extending it to allow for improved precision of parameter values, estimations of uncertainties, and statistical hypothesis testing. The basic workflow for the analysis follows:

1. Measure the value of the equilibrium constant between the blocked and closed states, K_B, using a stopped-flow kinetic technique (see Supporting Materials).
2. Perform steady-state fluorescence titrations measuring myosin binding to regulated thin filaments (RTFs; see Supporting Materials). The titrations should be carried out at three separate calcium concentrations (i.e., low, high, and intermediate calcium concentrations).
3. Normalize the data from each technical replicate before pooling the data.
4. Globally fit the pooled titration data set to determine the best fit parameters and calculate confidence intervals from bootstrapping simulations.
5. For a given perturbation, statistically test for differences between individual parameters obtained from the fitting.

A detailed user guide describing how to perform each of these steps, along with all of the data used to generate the figures in this manuscript is provided with the computational tool.

Results obtained using the traditional fitting procedure and the estimation of uncertainties

176 The individual equilibrium constants that define the positioning of cardiac
177 tropomyosin along the thin filament were determined using tissue-purified porcine cardiac
178 myosin and actin and recombinant human troponin and tropomyosin (see Supporting
179 Materials). The equilibrium constant for the transition between the blocked and closed
180 states, K_B, was determined by performing stopped-flow kinetic measurements. We
181 measured $K_B = 0.3 \pm 0.2$, in agreement with the previously determined value (4, 15).
182 Although there is some variance between technical replicates for K_B, the values of
183 parameters obtained from fitting of the titration data are relatively insensitive to small
184 changes in the value of K_B.

185 The equilibrium constants for the transition between the closed and open states,
186 K_T, and for myosin weak binding, K_W, were determined by performing titrations of RTFs
187 with myosin at high (pCa 3) and low (2 mM EGTA) calcium. The titration curves were fit
188 independently by Equation 1 (4). To ensure that the fitting was not biased by the initial
189 guesses of parameter values, we modified the fitting procedure described in (4) to
190 incorporate an annealing routine that iteratively fits the data with altered initial guesses.
191 The values obtained from these fits are shown in Figure 3A, and they are consistent with
192 values obtained previously with skeletal and cardiac muscle proteins (15-17). The original
193 formulation of the McKillop and Geeves model did not include a methodology for
194 determining uncertainty in fitted parameters. We developed a procedure to calculate 95%
195 confidence intervals via bootstrapping of the original data set (12, 13). With this
196 procedure, we saw that the classic approach gave considerable uncertainty in the values
197 of the fitted parameters. For example, for the data collected at low calcium, we obtained

198 uncertainties much larger than the measured parameters for both K_W (0.13 (-0.03/ +1.26))
199 and *nH* (6 (-2/+6)).
200
201 **Global fitting improves the resolution of fitted parameters**
202 To improve the resolution of parameters derived from the fitting of the data, we
203 adopted two modifications from the traditional approach. First, we performed an additional
204 titration at an intermediate calcium concentration (pCa 6.25). The inclusion of an
205 additional titration curve at an intermediate calcium is advantageous because some
206 perturbations shift the calcium sensitivity at intermediate calcium concentrations but not
207 under fully activating or deactivating conditions (18). Second, titration curves collected at
208 the three different calcium concentrations were fit globally rather than individually. In the
209 global fitting, the values of K_W, K_S, and *nH* were shared between the fits of all curves.
210 Global fitting of the three curves (Fig. 3A) yielded tighter 95% confidence intervals for
211 both K_W and *nH* (Fig. 3). The confidence interval for K_W was 0.13 (-0.02/+0.03), compared
212 to 0.13 (-0.03/+1.26) for the individually fit curve at low calcium. Similarly, the confidence
213 interval for *nH* for the individually fit data was 6 (-2/+6), while the confidence interval for
214 the globally fit data was 6 (-2/+4). These data demonstrate the improved resolution of this
215 approach.
216
217 **Hypothesis testing and its application to determining the biochemical mechanism**
218 **of a mutation that causes hypertrophic cardiomyopathy**
219 To demonstrate the utility of our approach for resolving the effects of molecular-
220 based changes in cardiac thin-filament regulation, we examined a point mutation that

221 causes familial hypertrophic cardiomyopathy (HCM), ΔE160 in troponin T (11). Clinical
222 studies have shown that this mutation causes pronounced ventricular hypertrophy and
223 sudden cardiac death, with half of the patients not surviving past age 40 (11). Previous
224 studies of the ΔE160 mutation in muscle fibers (19, 20), transfected myotubes (21), and
225 purified proteins (22) have shown that the ΔE160 mutation causes increased activation
226 of contractility. However, the biochemical mechanism of this activation is not well
227 understood.

228 We applied our methodology to determine which transitions involved in thin-
229 filament regulation (Fig. 1) are affected by the ΔE160 mutation. The goal of this analysis
230 is not an exhaustive characterization of the mutant; rather, it is to demonstrate the utility
231 of this approach for statistically assessing the effects of perturbations on thin-filament
232 regulation. From stopped-flow kinetic measurements (Fig. 4A), we obtained a K_B of 0.2 ±
233 0.1 for ΔE160, which is indistinguishable from the value obtained for wild-type (WT)
234 troponin (0.3 ± 0.2; p=0.41). We also performed fluorescence titrations (Fig. 4B) to
235 measure steady-state actomyosin binding and determine K_W, K_T, and nH. We used the
236 computational tool to calculate parameter values and their corresponding uncertainties
237 from global fitting of the titration curves (Fig. 4C).

238 To determine whether there are statistically significant differences between the
239 parameters for WT troponin and the ΔE160 mutant, we applied the hypothesis testing
240 methodology described in the Materials and Methods. We found that the mutant showed
241 a threefold increase in K_T at high calcium (0.17 (-0.12/+0.18) for WT versus 0.52 (-
242 0.16/+0.28) for ΔE160; p=0.014). This threefold increase in K_T would result in an
243 increased population of force-generating cross bridges at high calcium. We also found a

244 slight, but statistically significant, decrease in K_W (0.13 (-0.02/+0.03) for WT versus 0.08
245 (-0.01/+0.01) for ΔE160; p=0.002). We saw that at low calcium, K_T was 3-fold larger for
246 the mutant (p=0.076); however, this difference was not significant at the 95% confidence
247 level. We did not detect statistically significant differences in the values of *nH* (p=0.89),
248 K_B (p=0.41), or $K_{T\text{-}midcal}$ (p=0.95). The net effect of these changes would be to increase
249 activation, which is consistent with the hypercontractility associated with HCM. Taken
250 together, these data demonstrate the power of this approach for hypothesis testing and
251 for determining the biochemical mechanism of perturbations of thin-filament regulation.
252

253 **Application of the hypothesis testing and uncertainty estimation to other systems**

254 The computational tool for hypothesis testing and confidence interval estimation
255 from bootstrapping simulations is not limited to analysis of fluorescence titrations, but it
256 can be broadly applied to other data sets as well. We have supplied a stand-alone version
257 of this section of the code for examining the mean and median values (i.e., data frequently
258 used for single cell measurements) so that others can apply it to their experimental
259 system. This methodology is useful for data sets for which the form of the underlying
260 distribution is either unknown or not normal, such as single-molecule data (23) and single-
261 cell studies, as demonstrated in (18).
262

263 **Conclusion**

264 Here, we have demonstrated a method for extending the utility of the McKillop and
265 Geeves (4) approach to understanding thin-filament regulation, and we have provided a
266 well-documented, accessible computational tool to implement this methodology. Our

267 approach extends the McKillop and Geeves approach to include a method for calculating
268 confidence intervals and performing statistical tests. This methodology allowed us to
269 resolve the molecular effects of a mutation that causes hypertrophic cardiomyopathy. This
270 tool should be useful for studying physiological and pathological changes in muscle, as
271 well as for testing new therapies that target muscle regulation.
272

Code Availability

The computational tool can be downloaded from GitHub at:

https://github.com/GreenbergLab/Thin_Filament_Fitting

We also provide an in-depth user guide along with the raw data used in the examples presented here.

Acknowledgements:

Funding for this project was provided by the National Institutes of Health (R00HL123623, R01HL141086 to M.J.G., T32EB018266 to S.R.C.), and the March of Dimes Foundation (FY18-BOC-430198 to M.J.G.). We thank Tommy Blackwell and Tom Stump for critical evaluation of the code.

Conflict of interest statement:

All experiments were conducted in the absence of any commercial or financial relationships that could be construed as a potential conflict of interest.

Author contributions:

S.K.B. performed and analyzed the fluorescence experiments and developed code. S.R.C. helped with the early development and testing of the MATLAB code. L.G. generated mutant protein. M.J.G. oversaw the project and developed the early code for analyzing data. S.K.B. and M.J.G. wrote the first draft of the paper, and all authors contributed to the final draft.

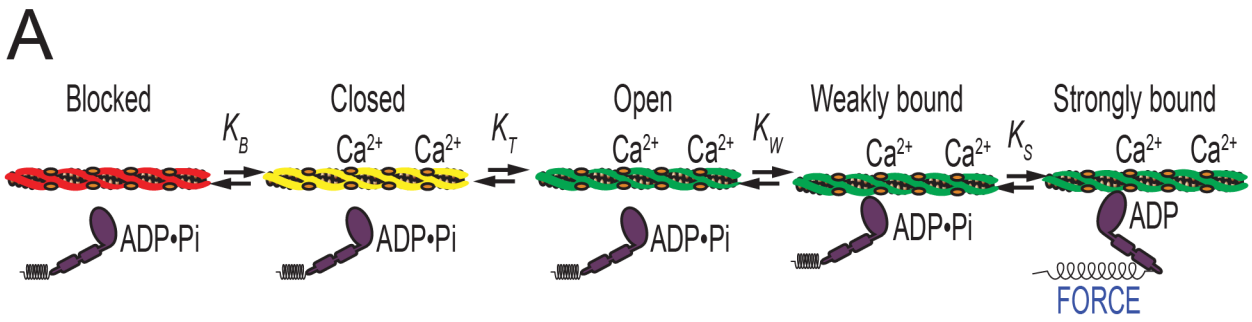

Figure 1. Schematic of the three-state model of muscle regulation. Red, yellow, and green represent the blocked, closed, and open states of tropomyosin, respectively. The equilibrium constants K_B and K_T describe transitions between states of tropomyosin on the thin filament, whereas K_W and K_S describe weak and strong myosin binding, respectively.

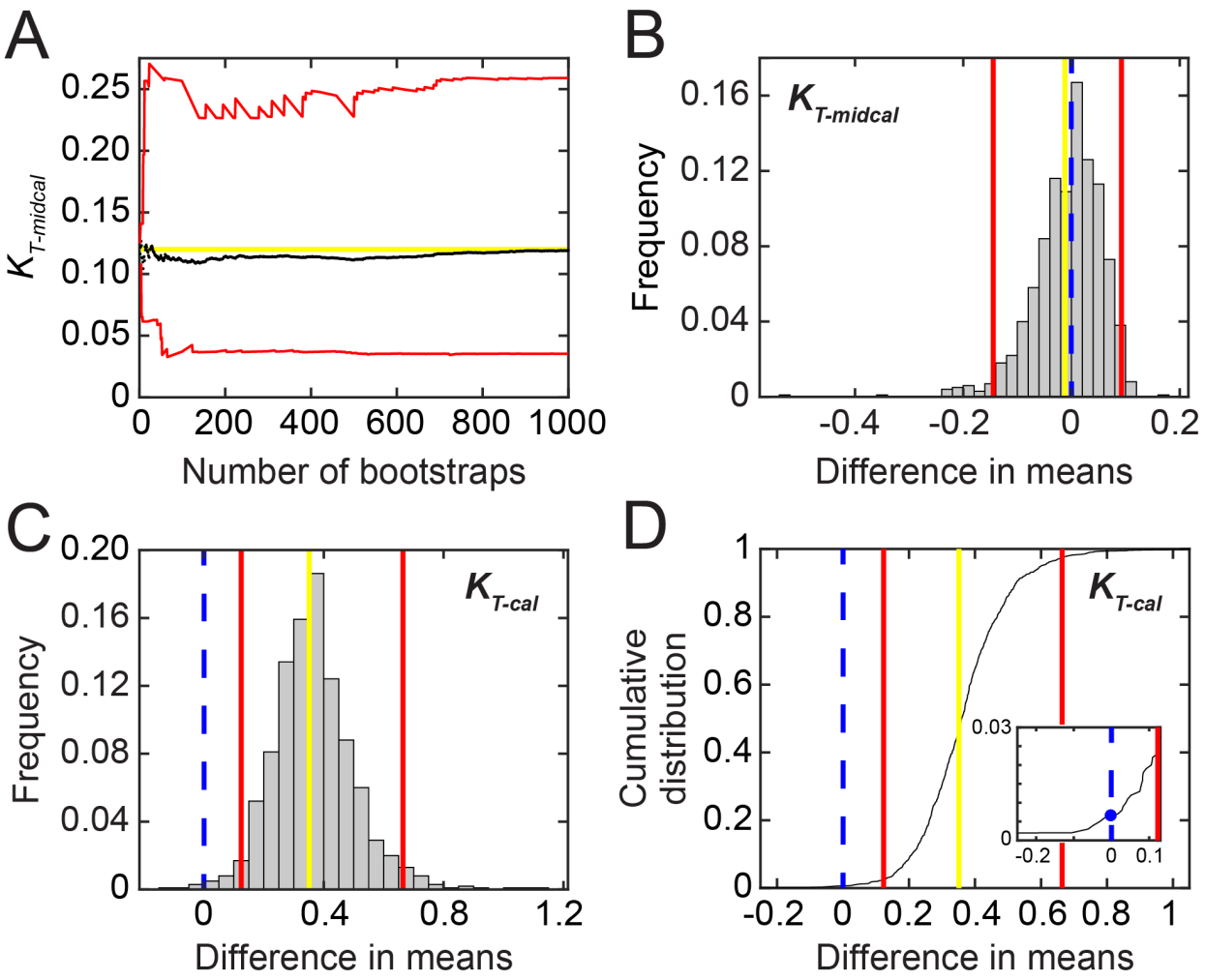

Figure 2. Hypothesis testing. **A.** Values of the average (black) and upper and lower bounds (red) of the 95% confidence interval for $K_{T\text{-}midcal}$ as a function of the number of bootstraps performed during error estimation. The yellow line marks the measured best-fit value. **B-C.** Histograms of the test statistic (i.e., the difference in means between parameters determined for WT and ΔE160) for $K_{T\text{-}midcal}$ (B) and $K_{T\text{-}cal}$ (C). Vertical lines represent the measured difference in means (yellow), the bounds of the 95% confidence interval (red), and the null hypothesis (blue dashed). The difference in parameter values is statistically significant at the 95% confidence level if the null hypothesis falls outside the 95% confidence interval, as in C. **D.** Cumulative distribution of the difference in means

317 between WT and ΔE160 calculated from the bootstrapping simulations for $K_{T\text{-}cal}$. Vertical
318 lines are the same as in C. Inset highlights the determination of the p-value (blue) from
319 the value of the cumulative distribution at x = 0. This value is multiplied by two to make
320 the test equivalent to a two-tailed test.
321
322

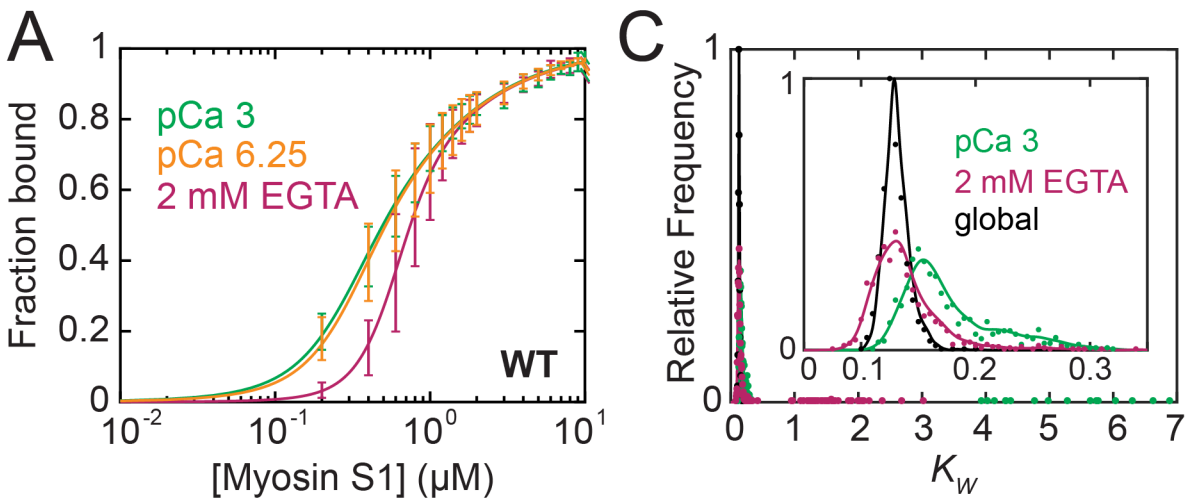

B

	2 mM EGTA Individual fit	pCa 3 Individual fit	Global fit
K_W	0.13 (-0.03/+1.26)	0.16 (-0.03/+0.13)	0.13 (-0.02/+0.03)
$K_{T\text{-}nocal}$	0.03 (-0.03/+0.07)	--	0.05 (-0.05/+0.09)
$K_{T\text{-}midcal}$	--	--	0.12 (-0.09/+0.13)
$K_{T\text{-}cal}$	--	0.22 (-0.21/+0.21)	0.17 (-0.12/+0.18)
n_H	6 (-2/+6)	4 (-1/+6)	6 (-2/+4)

Figure 3. Fitting the three-state model to fluorescence titration data. **A.** Steady-state titrations of regulated thin filaments with myosin for the WT protein conducted at three distinct calcium concentrations: saturating calcium (pCa 3, green), intermediate calcium (pCa 6.25, orange), and no calcium (2 mM EGTA, magenta). Curves are fits of the data. Error bars show the standard deviation of five technical replicates. **B.** Table of parameter values obtained from individual fits of data collected at 2 mM EGTA or pCa 3 compared to those obtained from our global fitting method, which includes pCa 6.25. Values in parentheses indicate the 95% confidence intervals. **C.** Histograms showing the frequency of K_W values determined from 1000 bootstrapping simulations. Points are the values from the global fitting (black) and from the individual fits of data collected at 2 mM EGTA (magenta) and pCa 3 (green). Lines are inserted to guide the eye. The inset shows the

distributions near the mean values of K_W. These data demonstrate that global fitting reduces the uncertainty in the measurement.

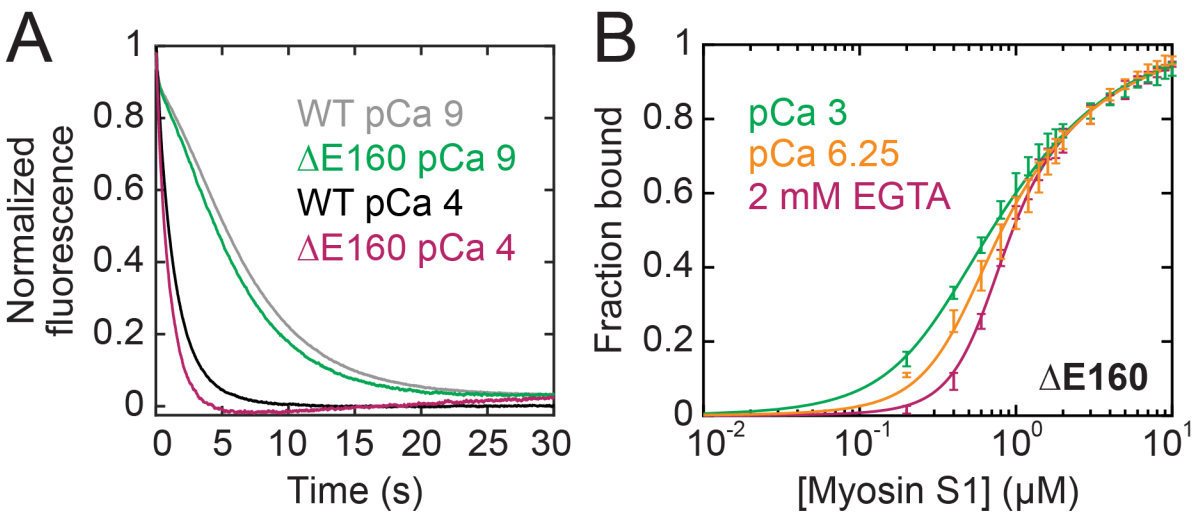

C

	WT (n=5)	**ΔE160** (n=5)	**p**
K_B	0.3 (+/- 0.2)	0.2 (+/- 0.1)	0.407
K_W	0.13 (-0.02/+0.03)	0.08 (-0.01/+0.01)	0.002*
$K_{T\text{-}nocal}$	0.05 (-0.05/+0.09)	0.15 (-0.07/+0.16)	0.076
$K_{T\text{-}midcal}$	0.12 (-0.09/+0.13)	0.11 (-0.04/+0.04)	0.950
$K_{T\text{-}cal}$	0.17 (-0.12/+0.18)	0.52 (-0.16/+0.28)	0.014*
n_H	6 (-2/+4)	6 (-1/+1)	0.888

Figure 4. Effects of ΔE160 mutation on thin-filament regulation. **A.** Normalized stopped-flow fluorescence traces of regulated thin filaments binding to myosin. The pyrene fluorescence is quenched at a higher rate at saturating calcium (pCa 4, magenta/black) than at low calcium (pCa 9, green/gray). The traces for WT (black/gray; average of n=6 curves each) and the ΔE160 mutant (magenta/green; average of n=4 curves each) are similar at each calcium concentration. **B.** Steady-state titrations of regulated thin filaments with myosin for the mutant protein conducted at three distinct calcium concentrations: saturating calcium (pCa 3, green), intermediate calcium (pCa 6.25, orange), and low calcium (2 mM EGTA, magenta). Curves are fits of the data. Error bars show the standard deviation of five technical replicates. **C.** Table of parameter values obtained for WT and ΔE160 troponin complexes from stopped-flow measurements (for K_B) and using the

351 computational tool (for all others). Values in parentheses indicate the 95% confidence

352 intervals. Asterisks indicate statistical significance at the 95% confidence level.

353

354

355

References

1. Malik, F. I., J. J. Hartman, K. A. Elias, B. P. Morgan, H. Rodriguez, K. Brejc, R. L. Anderson, S. H. Sueoka, K. H. Lee, J. T. Finer, R. Sakowicz, R. Baliga, D. R. Cox, M. Garard, G. Godinez, R. Kawas, E. Kraynack, D. Lenzi, P. P. Lu, A. Muci, C. Niu, X. Qian, D. W. Pierce, M. Pokrovskii, I. Suehiro, S. Sylvester, T. Tochimoto, C. Valdez, W. Wang, T. Katori, D. A. Kass, Y. T. Shen, S. F. Vatner, and D. J. Morgans. 2011. Cardiac myosin activation: a potential therapeutic approach for systolic heart failure. Science 331:1439-1443.
2. Green, E. M., H. Wakimoto, R. L. Anderson, M. J. Evanchik, J. M. Gorham, B. C. Harrison, M. Henze, R. Kawas, J. D. Oslob, H. M. Rodriguez, Y. Song, W. Wan, L. A. Leinwand, J. A. Spudich, R. S. McDowell, J. G. Seidman, and C. E. Seidman. 2016. A small-molecule inhibitor of sarcomere contractility suppresses hypertrophic cardiomyopathy in mice. Science 351:617-621.
3. Messer, A. E., and S. B. Marston. 2014. Investigating the role of uncoupling of troponin I phosphorylation from changes in myofibrillar Ca(2+)-sensitivity in the pathogenesis of cardiomyopathy. Front Physiol 5:315.
4. McKillop, D. F., and M. A. Geeves. 1993. Regulation of the interaction between actin and myosin subfragment 1: evidence for three states of the thin filament. Biophysical journal 65:693-701.
5. Lehman, W., R. Craig, and P. Vibert. 1994. Ca(2+)-induced tropomyosin movement in Limulus thin filaments revealed by three-dimensional reconstruction. Nature 368:65-67.
6. Woody, M. S., M. J. Greenberg, B. Barua, D. A. Winkelmann, Y. E. Goldman, and E. M. Ostap. 2018. Positive cardiac inotrope omecamtiv mecarbil activates muscle despite suppressing the myosin working stroke. Nat Commun 9:3838.
7. Gupta, M. P. 2007. Factors controlling cardiac myosin-isoform shift during hypertrophy and heart failure. Journal of molecular and cellular cardiology 43:388-403.
8. Garfinkel, A. C., J. G. Seidman, and C. E. Seidman. 2018. Genetic Pathogenesis of Hypertrophic and Dilated Cardiomyopathy. Heart Fail Clin 14:139-146.
9. Muthu, P., K. Kazmierczak, M. Jones, and D. Szczesna-Cordary. 2011. The effect of myosin RLC phosphorylation in normal and cardiomyopathic mouse hearts. Journal of cellular and molecular medicine.
10. Levine, R. J., Z. Yang, N. D. Epstein, L. Fananapazir, J. T. Stull, and H. L. Sweeney. 1998. Structural and functional responses of mammalian thick filaments to alterations in myosin regulatory light chains. Journal of structural biology 122:149-161.
11. Watkins, H., W. J. McKenna, L. Thierfelder, H. J. Suk, R. Anan, A. O'Donoghue, P. Spirito, A. Matsumori, C. S. Moravec, J. G. Seidman, and et al. 1995. Mutations in the genes for cardiac troponin T and alpha-tropomyosin in hypertrophic cardiomyopathy. The New England journal of medicine 332:1058-1064.
12. Efron, B. 1979. Bootstrap Methods: Another Look at the Jackknife. The Annals of Statistics 7:1-26.

13. Press, W. H. 1992. Numerical recipes in C : the art of scientific computing. Cambridge University Press, Cambridge England ; New York.
14. Martin, M. A. 2007. Bootstrap hypothesis testing for some common statistical problems: A critical evaluation of size and power properties. Comput Stat Data An 51:6321-6342.
15. Maytum, R., F. Bathe, M. Konrad, and M. A. Geeves. 2004. Tropomyosin exon 6b is troponin-specific and required for correct acto-myosin regulation. The Journal of biological chemistry 279:18203-18209.
16. Boussouf, S. E., R. Maytum, K. Jaquet, and M. A. Geeves. 2007. Role of tropomyosin isoforms in the calcium sensitivity of striated muscle thin filaments. Journal of muscle research and cell motility 28:49-58.
17. Maytum, R., B. Westerdorf, K. Jaquet, and M. A. Geeves. 2003. Differential regulation of the actomyosin interaction by skeletal and cardiac troponin isoforms. The Journal of biological chemistry 278:6696-6701.
18. Clippinger, S. R., P. E. Cloonan, L. Greenberg, M. Ernst, W. T. Stump, and M. J. Greenberg. 2019. Disrupted mechanobiology links the molecular and cellular phenotypes in familial dilated cardiomyopathy. Biorxiv.
19. Morimoto, S., Q. W. Lu, K. Harada, F. Takahashi-Yanaga, R. Minakami, M. Ohta, T. Sasaguri, and I. Ohtsuki. 2002. Ca(2+)-desensitizing effect of a deletion mutation Delta K210 in cardiac troponin T that causes familial dilated cardiomyopathy. Proceedings of the National Academy of Sciences of the United States of America 99:913-918.
20. Harada, K., F. Takahashi-Yanaga, R. Minakami, S. Morimoto, and I. Ohtsuki. 2000. Functional consequences of the deletion mutation deltaGlu160 in human cardiac troponin T. J Biochem 127:263-268.
21. Sweeney, H. L., H. S. Feng, Z. Yang, and H. Watkins. 1998. Functional analyses of troponin T mutations that cause hypertrophic cardiomyopathy: insights into disease pathogenesis and troponin function. Proceedings of the National Academy of Sciences of the United States of America 95:14406-14410.
22. Tobacman, L. S., D. Lin, C. Butters, C. Landis, N. Back, D. Pavlov, and E. Homsher. 1999. Functional consequences of troponin T mutations found in hypertrophic cardiomyopathy. The Journal of biological chemistry 274:28363-28370.
23. Woody, M. S., J. H. Lewis, M. J. Greenberg, Y. E. Goldman, and E. M. Ostap. 2016. MEMLET: An Easy-to-Use Tool for Data Fitting and Model Comparison Using Maximum-Likelihood Estimation. Biophysical journal 111:273-282.